Empirical parametrization for production cross sections of neutron-rich nuclei by photofission of ^{238}U at low energies

B. Mei,[1,2,*] D. L. Balabanski,[1] P. Constantin,[1] L. T. Anh,[1,3] and P. V. Cuong[1,4]

[1]*Extreme Light Infrastructure Nuclear Physics, "Horia Hulubei" National Institute for Physics and Nuclear Engineering, Str. Reactorului 30, 077125 Bucharest Magurele, Romania*

[2]*Institute of Modern Physics, Chinese Academy of Sciences, Lanzhou 730000, China*

[3]*Graduate University of Science and Technology, Vietnam Academy of Science and Technology, Hanoi 10000, Vietnam*

[4]*Centre of Nuclear Physics, Institute of Physics, Vietnam Academy of Science and Technology, Hanoi 10000, Vietnam*

(Received 10 August 2017; revised manuscript received 30 October 2017; published 18 December 2017)

An empirical parametrization for the production cross sections of ^{238}U photofission fragments at low energies ($E_\gamma < 30$ MeV) is developed. This parametrization, GIF^{238}U, consists of three parts, namely, the photofission cross section, the mass yield, and the isobaric charge distribution. The photofission cross section is parametrized to reproduce measured data over a wide energy range. The mass yield distribution is described by the energy-dependent multimodal fission model. The isobaric charge distribution is improved, relative to other parametrizations, to describe many experimental data sets over a broad mass range. Comparisons with different measured ^{238}U photofission data sets at various energies reveal that GIF^{238}U is in very good agreement with measured elemental and mass yields and can accurately reproduce experimental isotopic yields. Production cross sections (yields) of photofission fragments calculated by this parametrization indicate that many neutron-rich nuclei approaching the r-process path can be accessed via photofission of ^{238}U at radioactive-beam facilities.

DOI: 10.1103/PhysRevC.96.064610

I. INTRODUCTION

Photofission reactions, and in particular low energy photofission reactions, have been widely investigated for several decades. In previous studies, photofission cross sections [1–4] as well as the mass [5,6] and charge [7] distributions in the low energy photofission of actinide targets, especially ^{238}U, have been measured using photons mainly from bremsstrahlung and other methods. These photofission studies are very important not only for understanding the photofission mechanism but also for exploring nuclear structure effects [8,9]. Recently, there has been growing interest in photofission, because it provides one of most powerful methods for producing neutron-rich exotic nuclei close to the r-process path. Some present and future radioactive-beam facilities are based on photofission of actinide targets [10]. For instance, photofission of uranium targets has been or will be used at the ALTO facility at IPN Orsay [11], the DRIBs at JINR [12], the ARIEL facility at TRIUMF [13], the ANURIB at VECC [14], and the IGISOL facility at ELI-NP [8,15,16]. Most of the above facilities are based on the bremsstrahlung technique, while the γ beam at ELI-NP will be produced by laser Compton backscattering. A similar Compton backscattering method has been successfully applied to study photofission reactions at the HIγS facility at Duke University [3]. In addition, photofission reactions play an important role in producing medical isotopes [17], reprocessing of nuclear waste [18], and many other technical applications.

For producing neutron-rich nuclei, designing nuclear physics experiments, and many other applications, an accurate calculation for production cross sections of photofission fragments is crucial. Calculations for these cross sections in ^{238}U photofission at low energies over the whole giant dipole resonance (GDR) region are of specific interest for estimating the production yields of neutron-rich fragments and optimizing nuclear physics experiments at the above mentioned facilities [8,11–16]. General fission models, e.g., GEF [19] and FIPRODY [20], have been developed for predicting the manifold fission observables in various fission systems, however, their predictive power for production yields of ^{238}U photofission fragments is not validated. Since calculations by these statistical fission models can be very time consuming, a fast and accurate empirical parametrization for production cross sections of fragments produced by ^{238}U photofission at low energies is particularly useful. Recently, an empirical parametrization [21,22], based on the mass yields measured at the average photon energy of 13.7 MeV [6], has been proposed to calculate production cross sections of fragments produced by photofission of ^{238}U at 13.7 MeV. However, this parametrization cannot be used to describe the mass yields at other energies below 30 MeV, especially for the fission modes with a strong energy dependence such as the symmetric mode, according to the mass yields measured at different excitation energies [5,6]. In addition, the total photofission cross section in this parametrization is fitted to limited experimental data between 7.8 and 18.3 MeV [4], therefore it cannot reproduce the small photofission cross sections measured at lower energies below about 6 MeV [3]. As far as we know, an accurate empirical parametrization based on the ^{238}U photofission data measured over a wide energy range below 30 MeV is still lacking, and thus there is a need to develop a reliable empirical parametrization for the above mentioned applications.

In the present work, an empirical parametrization, called GIF^{238}U, is proposed to accurately calculate production cross

*bo.mei@eli-np.ro

sections of neutron-rich nuclei produced by γ-induced fission of ^{238}U at low energies ($E_\gamma < 30$ MeV). This parametrization consists of three components: the total photofission cross section, the mass yield distribution, and the isobaric charge distribution. The parametrization of the total photofission cross section is developed by fits to several experimental data over a wide energy range. The mass yield distribution is constructed on the basis of the multimodal fission model [9], while the energy dependence is also taken into account in the parametrization of the mass yield. The isobaric charge distribution is determined by comparing with extensive experimental data. In the following, different parts used in the GIF^{238}U parametrization will be described separately. To study the validity as well as the overall quality of GIF^{238}U, calculations based on this parametrization will be compared with many experimental data. Finally, production cross sections of many neutron-rich exotic nuclei ($26 \leqslant Z \leqslant 65$), produced by ^{238}U photofission, will be calculated by using this new parametrization.

II. FORMULA FOR PRODUCTION CROSS SECTIONS OF PHOTOFISSION FRAGMENTS

The production cross section of a specific fragment with mass number A and nuclear charge Z produced by ^{238}U photofission can be calculated by the following analytical formula:

$$\sigma(A,Z) = \sigma_f(E_\gamma)Y(A,Z)/100. \quad (1)$$

$\sigma_f(E_\gamma)$ is the photofission cross section at an incident photon energy E_γ and $Y(A,Z)$ represents the independent yield per 100 photofission events. In the following, details of different terms in Eq. (1) will be discussed separately.

A. Total photofission cross sections

^{238}U photofission cross sections at different energies have been measured in various experiments [1–4]. According to Ref. [21], photofission cross sections between 7.8 and 18.3 MeV can be well described by Lorentz distributions; however, this analysis is restricted to a limited energy range. In the present work, the energy range is increased and ^{238}U photofission cross sections between 5.93 and 30 MeV (above the fission barrier) are parametrized by the sum of two Lorentz functions:

$$\sigma_f(E_\gamma) = \sum_{i=1}^{2} \frac{\sigma_i}{1+\left[\frac{(E_\gamma^2-E_i^2)}{E_\gamma\Gamma_i}\right]^2}. \quad (2)$$

σ_i, E_i, and Γ_i are the peak height, resonance energy, and full width at half maximum, respectively, which are determined by fitting the photofission cross sections above 5.93 MeV measured in Refs. [1,2]. Photofission cross sections at energies higher than 30 MeV cannot be described by Lorentz functions [23] and for this reason are not included in this work. Photofission cross sections at energies $E_\gamma < 5.93$ MeV (bellow the fission barrier) are parametrized as

$$\sigma_f(E_\gamma) = t_1 \exp[-(E_\gamma - t_2)^2/t_3]. \quad (3)$$

TABLE I. The values of constants used in the empirical parametrization for ^{238}U photofission.

Parameter	Constant	Value
High energy photofission cross section σ_f^{HE}	σ_1	59.39
	E_1	10.71
	Γ_1	1.9394
	σ_2	169.586
	E_2	14.4136
	Γ_2	5.0806
Low energy photofission cross section σ_f^{LE}	t_1	23.9285
	t_2	7.08
	t_3	0.9851
Symmetric mode SM $C_{\rm SM}$	c_1	0.021
	c_2	0.21
Symmetric mode SM $\sigma_{\rm SM}$	w_1	0.437
	w_2	−0.5337
Asymmetric mode ASMI $C_{\rm ASMI}$	c_3	32.095
	c_4	0.947
Asymmetric mode ASMI $\sigma_{\rm ASMI}$	$\sigma_{\rm ASMI}$	2.23
Asymmetric mode ASMII $C_{\rm ASMII}$	$C_{\rm ASMII}$	5.55
Asymmetric mode ASMII $\sigma_{\rm ASMII}$	$\sigma_{\rm ASMII}$	5.8
Peak positions of 3 modes	$A_{\rm SM}$	117.35
	$D_{\rm ASMI}$	15.78
	$D_{\rm ASMII}$	21.8
$Z_{\rm prob}$ correction Δ_Z	d_1	32.452
	d_2	−0.957
	d_3	9.42×10^{-3}
	d_4	-3.09×10^{-5}
	d_5	0.373
	d_6	−4746.9
	d_7	−16.418
Charge width C_p	C_p	0.85

Values of the parameters t_1, t_2, and t_3 are obtained by fitting Eq. (3) to the low energy experimental data measured in Ref. [3] and are shown in Table I.

Figure 1 presents the comparison of ^{238}U photofission cross sections measured in Refs. [1–3] with calculations by Eqs. (2) and (3) used in this parametrization as well as a fit to the above experimental data using only Eq. (2). It is obvious that our parametrization is in very good agreement with experimental data over a wide energy range, despite a small discrepancy around 6.1 MeV, which may be caused by a small sub-barrier resonance. However, Eq. (2) significantly overestimates the ^{238}U photofission cross section below about 5.9 MeV, as shown by the dotted line in Fig. 1.

B. Mass yields

Based on the multimodal fission model [9], the mass distribution of photofission fragments can be written as a sum of contributions from three different fission modes, namely, one symmetric mode (SM) and two asymmetric modes (ASMI and ASMII). The contribution of each mode is determined by the probability of passing through the fission barrier of a specific shape, which may depend on the photon energy. For the symmetric mode the mass yield can be described in the form of a Gaussian function peaked around $A \approx 117$,

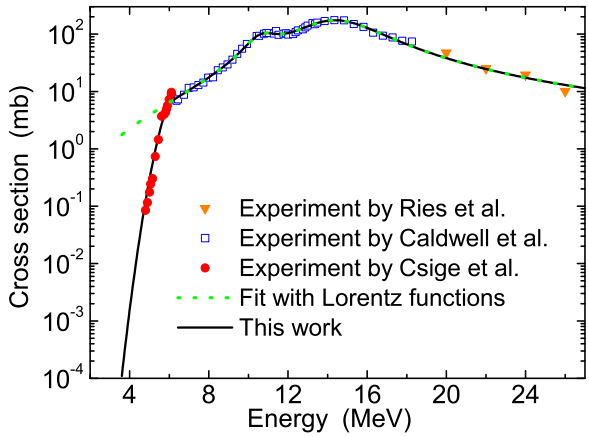

FIG. 1. The ^{238}U photofission cross sections measured by Caldwell *et al.* [1], Ries *et al.* [2], and Csige *et al.* [3], as a function incident photon energy. The relative uncertainty is less than 20% for most of the measured data. The full line indicates calculations by the parametrization used in this work based on Eqs. (2) and (3), whereas the dotted line represents a fit of Eq. (2) to measured photofission cross sections.

while two Gaussian functions are required for describing each asymmetric mode. Therefore the total yield of photofission fragments with a given mass number A (per 100 photofission events) can be described by the sum of five Gaussian functions:

$$\begin{aligned} Y(A) &= Y_{\rm SM}(A) + Y_{\rm ASMI}(A) + Y_{\rm ASMII}(A) \\ &= C_{\rm SM}\exp\left[-\frac{(A-A_{\rm SM})^2}{2\sigma_{\rm SM}^2}\right] \\ &\quad + C_{\rm ASMI}\exp\left[-\frac{(A-A_{\rm SM}-D_{\rm ASMI})^2}{2\sigma_{\rm ASMI}^2}\right] \\ &\quad + C_{\rm ASMI}\exp\left[-\frac{(A-A_{\rm SM}+D_{\rm ASMI})^2}{2\sigma_{\rm ASMI}^2}\right] \\ &\quad + C_{\rm ASMII}\exp\left[-\frac{(A-A_{\rm SM}-D_{\rm ASMII})^2}{2\sigma_{\rm ASMII}^2}\right] \\ &\quad + C_{\rm ASMII}\exp\left[-\frac{(A-A_{\rm SM}+D_{\rm ASMII})^2}{2\sigma_{\rm ASMII}^2}\right]. \end{aligned} \quad (4)$$

The Gaussian parameters $C_{\rm SM}$, $C_{\rm ASMI}$, $C_{\rm ASMII}$ and $\sigma_{\rm SM}$, $\sigma_{\rm ASMI}$, $\sigma_{\rm ASMII}$ are the amplitudes and widths, respectively, of the symmetric (SM) and two asymmetric (ASMI and ASMII) fission modes. $A_{\rm SM}$ is the most probable mass number for the symmetric fission mode. $A_{\rm SM} - D_{\rm ASMI}$ and $A_{\rm SM} + D_{\rm ASMI}$ ($A_{\rm SM} - D_{\rm ASMII}$ and $A_{\rm SM} + D_{\rm ASMII}$) are the most probable mass numbers of the light and heavy fragments, respectively, for the asymmetric mode ASMI (ASMII). These Gaussian parameters can be determined by fitting Eq. (4) to measured mass yields [5,6] over a wide energy range, as shown in Fig. 2. According to these experimental data, the most probable mass numbers are almost constants at different energies for three fission modes and thus $A_{\rm SM}$, $D_{\rm ASMI}$, and $D_{\rm ASMII}$ are energy independent. The amplitude and width of the asymmetric mode ASMII as well as the width of the asymmetric mode ASMI also come out as energy independent. However, the contribution of the symmetric fission mode decreases rapidly as the photon energy decreases, as shown by data points in the mass range $107 < A < 127$ in Fig. 2.

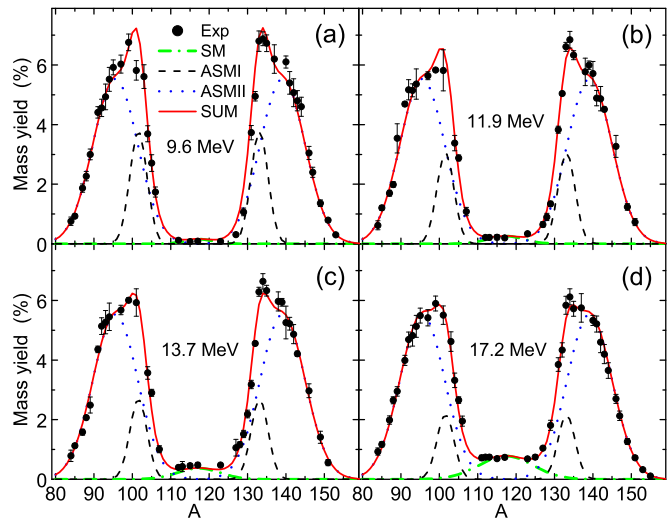

FIG. 2. Measured mass yields for ^{238}U photofission by bremsstrahlung photons with endpoint energies 12, 19.5, 29.1, and, 70 MeV [5,6]. The corresponding average photon energies are (a) 9.6, (b) 11.9, (c) 13.7, and (d) 17.2 MeV [6]. The full lines indicate fits by Eq. (4). The symmetric mode (SM) (dash-dotted lines) as well as the asymmetric modes ASMI (dashed lines) and ASMII (dotted lines) are also shown.

Within the GIF^{238}U parametrization, the amplitude and width of the symmetric mode as well as the amplitude of the asymmetric mode ASMI depend on the photon energy E_γ. The amplitude of the symmetric mode is parametrized as

$$C_{\rm SM} = c_1\exp(c_2 E_\gamma), \quad (5)$$

and the width of the symmetric mode is expressed as

$$\sigma_{\rm SM} = w_1 E_\gamma + w_2. \quad (6)$$

The amplitude of the asymmetric mode ASMI is parametrized as

$$C_{\rm ASMI} = c_3 E_\gamma^{-c_4}. \quad (7)$$

In Fig. 2, the mass yield distributions calculated by this parametrization are compared with those measured at different energies in Refs. [5,6]. The average energy of bremsstrahlung photons [6] is used in the above calculations of the mass yield. Calculated mass yields are in very good agreement with experimental data measured at different energies. Contributions from different fission modes (SM, ASMI, and ASMII) are also indicated in Fig. 2 by dash-dotted, dashed, and dotted lines.

C. Isobaric charge distributions

After the mass yield has been determined, one can calculate the independent yield of the photofission fragment with the given A and Z (per 100 photofission events) with the following

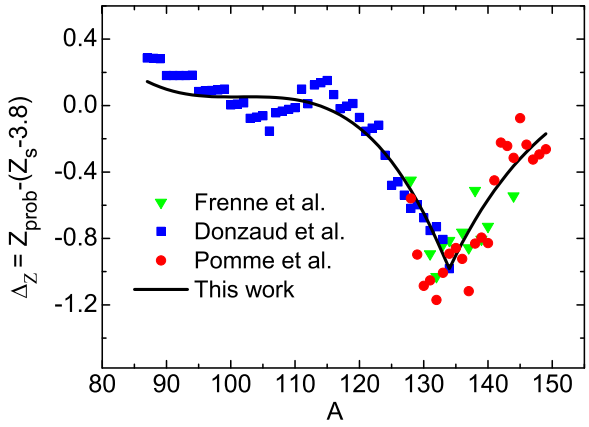

FIG. 3. Difference between the most probable charge $Z_{\rm prob}$ from experimental data measured by Donzaud *et al.* [24], Frenne *et al.* [25], as well as Pommé *et al.* [26] and $(Z_s - 3.8)$ proposed in Ref. [21]. The error is less than 0.2 for most of the experimental data. The black solid line is the correction factor Δ_Z calculated by Eqs. (11) and (12).

expression:

$$Y(A,Z) = \frac{Y(A)}{\sqrt{\pi C_p}} \exp\left[-\frac{(Z - Z_{\rm prob})^2}{C_p}\right], \tag{8}$$

where the isobaric charge distribution of photofission products with a given mass A is approximated by using a Gaussian function. $Z_{\rm prob}$ is the most probable charge number of fission fragments with a given mass A, while C_p indicates the width of the charge distribution for the isobaric chain. The mass yield $Y(A)$ is calculated by Eq. (4).

According to Ref. [21], the most probable charge number $Z_{\rm prob}$ can be approximated by $(Z_s - 3.8)$. Z_s represents the most stable isotope of fission fragments with mass number A and can be derived from the liquid drop model mass formula:

$$Z_s = \frac{A + [(a_c A^{2/3})/(2x)]}{(4a_{\rm sym}/x) + [(a_c A^{2/3})/x]}, \tag{9}$$

where $x = 2a_{\rm sym} + [(m_n - m_p)/2]$, and m_n and m_p are the masses of proton and neutron, respectively [27]. The constants $a_c = 0.71$ MeV and $a_{\rm sym} = 23.21$ MeV are the Coulomb and symmetry energy coefficients, respectively [21,27]. Since the above approximation for $Z_{\rm prob}$ is based on very limited experimental data around $A = 97$, its validity should be checked by comparing with more experimental data. This is done in Fig. 3 by comparing the difference between the most probable charge number $Z_{\rm prob}$ from many measured ^{238}U photofission data [24–26] and the above most probable charge number $(Z_s - 3.8)$ proposed in Ref. [21]. It is clear that the above approximation is only valid for fission fragments around $A = 97$, where $Z_{\rm prob} \approx (Z_s - 3.8)$. However, there are very large differences for the fission fragments around $A = 134$, and thus significant deviations may occur when the above approximation is applied for calculations of fission fragment cross sections.

To reproduce the experimental data [24–26] over a broad range of fragment mass, the most probable charge number $Z_{\rm prob}$ in this study is improved by introducing a correction term Δ_Z,

$$Z_{\rm prob} = Z_s - 3.8 + \Delta_Z, \tag{10}$$

where Z_s is calculated by Eq. (9). The correction term Δ_Z is parametrized as

$$\Delta_Z = d_1 + d_2 A + d_3 A^2 + d_4 A^3, \tag{11}$$

for light fragments with $A < 134$, and as

$$\Delta_Z = d_5 + d_6 \exp(A/d_7), \tag{12}$$

for heavy fragments with $A \geqslant 134$. This parametrization of the correction term Δ_Z is in good agreement with several ^{238}U photofission measurements [24–26], as shown in Fig. 3. The minimum value of Δ_Z occurs around $A = 134$, and $Z_{\rm prob} = 52$ and thus the most probable neutron number $N_{\rm prob} = 82$, which is due to the strong impact of the closed neutron shell 82.

The width parameter C_p in Eq. (8) is found to be almost constant, $C_p = 0.85$, which has been determined by comparing the independent yields of photofission fragments calculated by Eq. (8) with many experimental data for ^{238}U photofission induced by virtual photons [24] with an average excitation energy around 18 MeV, as described below. This C_p value is also in excellent agreement with that used in many other works [6,21].

The values of various constants used in the above equations are listed in Table I. Since there is no experimental data to constrain these parameters at extremely low energies, the GIF^{238}U parametrization is restricted to the ^{238}U photofission reactions above about 4 MeV.

III. COMPARISONS WITH EXPERIMENTAL DATA AND GEF CALCULATIONS

In order to evaluate the validity of the above parametrization and its parameters, one can compare the calculations by this parametrization with the elemental, mass, and isotopic yields measured in ^{238}U photofission experiments. In Fig. 4, the comparison of the elemental yields $Y(Z) = \Sigma_A Y(A,Z)$ measured in two ^{238}U photofission experiments at different average excitation energies [7,24] with the calculations by the GIF^{238}U parametrization is shown. The calculated elemental yields are in excellent agreement with the two experimental data within the uncertainties. In the atomic number range $43 \leqslant Z \leqslant 49$, there are large differences between the elemental yields calculated for two experiments at different average excitation energies, which is mainly caused by the different contributions from the symmetric fission mode at different excitation energies (see also Fig. 2). Thus, high energy photons are required in order to enhance the independent yields of photofission fragments with $43 \leqslant Z \leqslant 49$ and $107 < A < 127$, as shown in Figs. 4 and 2.

To continue the validation of GIF^{238}U, the mass yields measured in inverse kinematics at two different projectile energies via the virtual photon induced fission of ^{238}U [24,28] are also compared with the mass yields calculated by this parametrization. As shown in Fig. 5, the calculated and measured mass yields are in good agreement for both experiments. Based on these comparisons, the average excitation energies in GIF^{238}U calculations are estimated to be 18 ± 0.9 and 16.5 ± 0.8 MeV

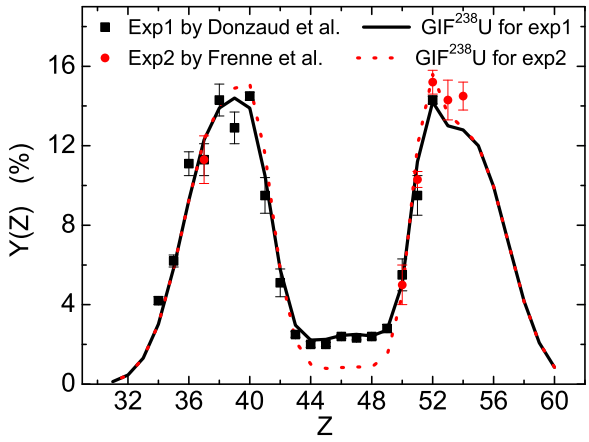

FIG. 4. Elemental yields $Y(Z) = \Sigma_A Y(A,Z)$ measured in two ^{238}U photofission experiments [7,24]. The black solid and red dotted lines represent the calculations by the GIF^{238}U parametrization for two ^{238}U photofission experiments at average excitation energies around 18 MeV measured by Donzaud *et al.* [24] and 13 MeV measured by Frenne *et al.* [7], respectively.

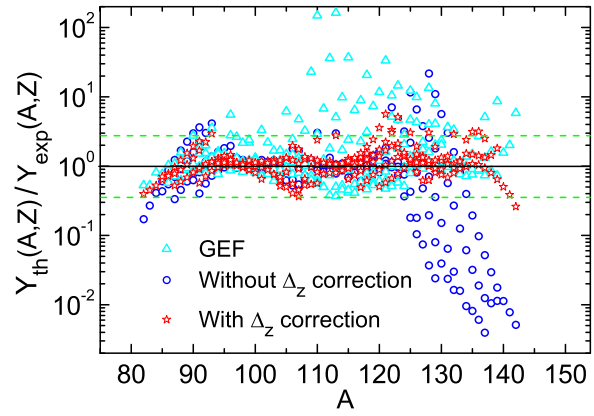

FIG. 6. Ratio of independent yields of ^{238}U photofission fragments $Y(A,Z)$ calculated by the GEF code [19] (open triangles) as well as the GIF^{238}U parametrization when the correction factor Δ_Z is applied for $Z_{\rm prob}$ (open stars) and that without Δ_Z correction (open circles) to the experimental data in Ref. [24]. For the case of GIF^{238}U calculations with Δ_Z correction, 95% of data are distributed between two dashed green lines, corresponding to the range of $\pm 2\sigma$.

for two experiments in panels (a) [24] and (b) [28] of Fig. 5, respectively. These values also agree well with the average excitation energies of 19 and 15.2 ± 1.0 MeV estimated in Refs. [24] and [28], respectively, according to peak-to-valley ratios in their measured mass yield distributions.

The validity of this new empirical parametrization can be visualized in the ratios of calculations using the parametrization to experimental data. For this purpose, Fig. 6 represents ratios between the independent yields of photofission fragments $Y(A,Z)$ calculated by the GIF^{238}U parametrization with

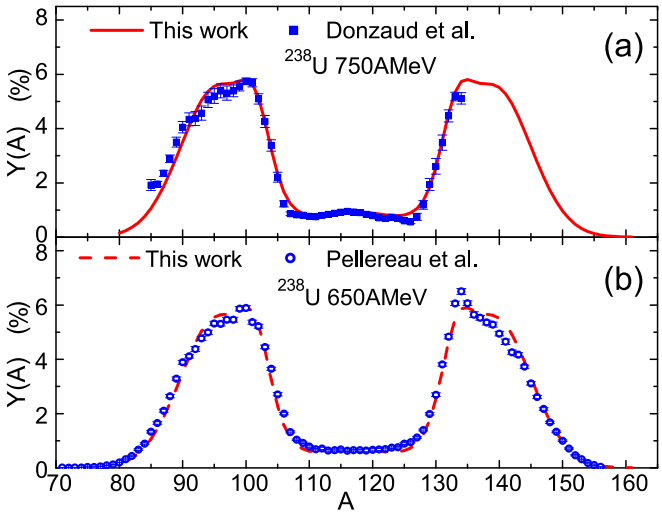

FIG. 5. Comparison between the mass yields measured in two experiments at GSI via the virtual photon induced fission of ^{238}U [24,28] and those calculated by the GIF^{238}U parametrization in this work. In these experiments, the virtual photon induced fission reactions have been measured by 750A[24] and 650A MeV [28] ^{238}U impinging on heavy targets (Pb target used by Donzaud *et al.* in Ref. [24]; Pb and U targets used by Pellereau *et al.* in Ref. [28]).

the correction term Δ_Z in $Z_{\rm prob}$ and the experimental data from Ref. [24], where measured fragments from low energy photofission were selected and identified by their magnetic rigidities. As shown in Fig. 6, 95% of the ratio values ($Y_{\rm th}/Y_{\rm exp}$) are distributed from about 0.35 to 2.8, corresponding to the range of $\pm 2\sigma$. For comparison, we also show with open circles the ratios when the correction term Δ_Z is not taken into account in the parametrization. A significant discrepancy is observed for the calculations neglecting the correction term Δ_Z in Eq. (10), especially in the mass range $125 \leqslant A \leqslant 145$, where the magnitude of Δ_Z is large, as shown in Fig. 3. This comparison indicates that the correction term Δ_Z should be considered in the GIF^{238}U parametrization to accurately calculate the production yields of ^{238}U photofission fragments. Figure 6 also displays the ratios calculated by a general fission model GEF [19], where the aforementioned average excitation energy estimated in Ref. [24] is used in GEF calculations. As shown by open triangles in Fig. 6, large discrepancies are observed in GEF calculations [19] for some isotopes in the mass range $105 \leqslant A \leqslant 130$.

Furthermore, the overall quality of the above empirical parametrization GIF^{238}U and the GEF model can be quantitatively evaluated by the rms deviation factor defined via the following equation [29–31]:

$$f_{\rm rms} = \exp\left[\frac{1}{N}\sum_{i=1}^{N}\left(\ln\frac{Y^i_{\rm th}(A,Z)}{Y^i_{\rm exp}(A,Z)}\right)^2\right]^{1/2}, \qquad (13)$$

where N is the number of independent yields of isotopes measured in Ref. [24] (about 230). According to Eq. (13), independent yields of ^{238}U photofission fragments are reproduced by the GIF^{238}U parametrization within a factor of 1.6, namely, $f_{\rm rms} = 1.6$, which is much smaller than the value of 2.9 for GEF. The remarkably good agreement between calculations by the GIF^{238}U parametrization and many experimental data measured in Ref. [24] supports that this parametrization is very

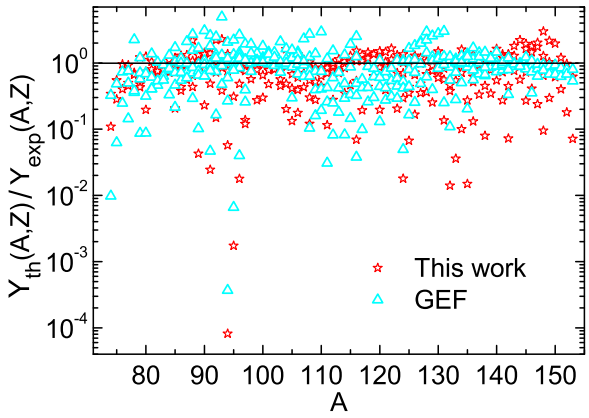

FIG. 7. Ratio between independent yields calculated by the GIF^{238}U parametrization with Δ_Z correction for Z_{prob} (open stars) as well as the GEF calculations [19] with an average excitation energy of 15.2 MeV (open triangles) and the experimental data measured in Ref. [28].

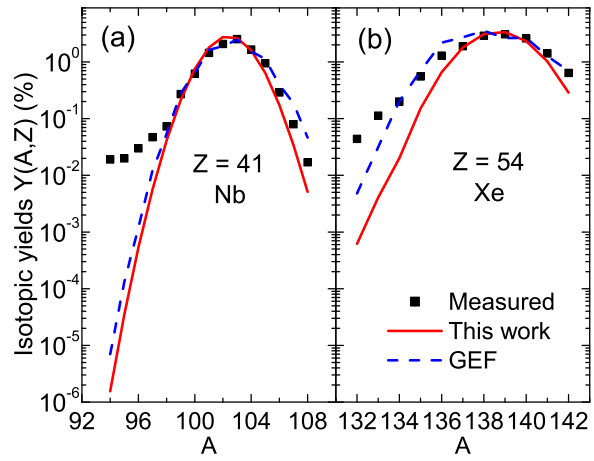

FIG. 8. Typical example of comparison between the isotopic yields calculated by the GEF code [19] (dashed lines) as well as the GIF^{238}U parametrization (full lines) and those measured in Ref. [28] for isotopes with $Z = 41$ and 54. The relative uncertainty is reported to be less than 20% for most of the experimental data [28].

suitable for a fast and accurate estimate of production cross sections (yields) of the ^{238}U photofission fragments.

In another recent experiment, independent yields of isotopes from the virtual photon induced fission of ^{238}U were measured by 650A MeV ^{238}U projectiles impinging on heavy targets (Pb and U) [28]. The experimental setup in this experiment does not allow one to disentangle events produced by the virtual photon induced fission from those produced by fragmentation reactions. The subtraction of the fragmentation induced background in Ref. [28] is based on the limiting fragmentation hypothesis: fragmentation induced distributions in the fragment charge, mass, and excitation energy are independent of the target and beam energy. However, many measured fragmentation data reveal that this limiting fragmentation hypothesis can be questioned (see, e.g., Ref. [29] and references therein). Isotopic yields measured in this experiment [28] are also compared with calculations by the GIF^{238}U parametrization and the GEF code [19], as shown in Fig. 7. Although most measured and calculated yields are in reasonable agreement, significant deviations up to orders of magnitude are observed for yields of many isotopes very close to the stability line, according to calculations by both GIF^{238}U and GEF. As a typical example, Fig. 8 shows the comparison between isotopic yields calculated by the GIF^{238}U parametrization as well as the GEF code [19] and those measured in Ref. [28] for isotopes with $Z = 41$ and 54. The peak position and the right wing of the distribution can be well described by the GIF^{238}U parametrization and GEF. However, large deviations from the Gaussian function are observed in Fig. 8 for yields of isotopes on the left wing of the distribution, especially for those isotopes very close to the stability line, where the contribution from the fragmentation induced background is significant but that from the virtual photon induced fission is very small [8,29]. It should be pointed out that these significant deviations in Figs. 7 and 8 have almost no impact on mass yields in panel (b) of Fig. 5, because these deviations occur only for fragments with very small isotopic yields in photofission. Furthermore, many isotopic yields measured in the proton- and deuterium-induced fission of ^{238}U [32,33] support that the isotopic yield distribution can be well reproduced by a Gaussian function. The above evidence suggests that deviations of the experimental data in Ref. [28] from calculations based on the GIF^{238}U parametrization as well as GEF shown in Figs. 7 and 8 are related to background contributions from fragmentation reactions. The above deviations should be eliminated when the fragmentation induced background is unambiguously subtracted by improving the experimental technique with an event-by-event identification of measured fragments on one side and accurately modeling the fragmentation background on the other side.

IV. CALCULATIONS FOR PRODUCTION CROSS SECTIONS OF NEUTRON-RICH NUCLEI

Many experiments at present and future radioactive-beam facilities aim at producing and investigating the neutron-rich exotic nuclei, especially those close to the r-process path, by means of ^{238}U photofission at different energies. It is essential to accurately calculate production cross sections (rates) of these neutron-rich exotic nuclei for such experiments. For this purpose, one can calculate production cross sections of the neutron-rich nuclei by using the GIF^{238}U parametrization proposed in this work. As an example, Fig. 9 shows the calculated cross sections of neutron-rich fragments produced by photofission of ^{238}U using 14 MeV photons. The calculated results demonstrate clearly that the ^{238}U photofission is particularly suitable for producing many neutron-rich exotic nuclei with $31 \leqslant Z \leqslant 62$ and $80 \leqslant A \leqslant 160$. For many neutron-rich nuclei on or close to the r-process path [34], a production cross section of the order of about 1 mb can be achieved by using ^{238}U photofission at low energies. For instance, it is interesting to notice that production cross sections of $^{80-82}$Ge and $^{85-87}$Se around the closed shell $N = 50$ are about 0.17 and 1.1 mb, respectively, while production cross sections of ^{132}Sn and ^{134}Te around the closed shell $N = 82$ are roughly 0.66 and 6.4 mb,

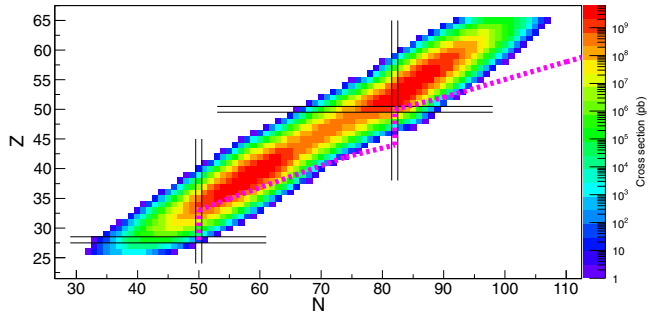

FIG. 9. Cross sections of fragments produced by photofission of ^{238}U using 14 MeV photons, calculated by the GIF^{238}U parametrization. The dotted lines illustrate the position of the r-process path [34]. The proton and neutron closed shells are indicated with the black solid lines.

respectively. The above cross sections calculated with GIF^{238}U can be applied to estimate the production rates of neutron-rich nuclei produced by ^{238}U photofission and optimize nuclear physics experiments. As an example, production rates of ^{132}Sn and ^{134}Te in ^{238}U targets with a total thickness of 251 μm are about 2×10^4 and 2×10^5 ions/s, respectively, according to calculations by GIF^{238}U for the IGISOL facility at ELI-NP. In this calculation, the total intensity of the gamma beam (with a broad energy distribution between 10 and 18.5 MeV) is conservatively estimated to be 5×10^{10} γ/s at the γ production point, while ^{238}U targets (about 33 foils tilted at 15°) are placed around 7 m after this γ production point [8,15,16]. More detailed calculations by GIF^{238}U for the planned IGISOL facility at ELI-NP will be addressed in future works.

It should be mentioned that many neutron-rich exotic nuclei can also be produced by other nuclear reaction mechanisms. For instance, the projectile fragmentation reactions at high energies have also been used to produce both neutron- and proton-rich fragments at many radioactive-beam facilities [29,35–39].

V. SUMMARY

An empirical parametrization, called GIF^{238}U, is proposed for accurately calculating production cross sections (yields) of neutron-rich fragments produced by photofission of ^{238}U over a wide energy range. This parametrization consists of the total photofission cross section, the mass yield, and the isobaric charge distribution. The formulas for the total photofission cross section can reproduce the experimental data over a wide energy range (below about 30 MeV). The mass yield distribution is based on the multimodal fission model, while an energy dependence is introduced according to the mass yield distributions measured at different energies. Furthermore, a correction term is included for the most probable charge number to reproduce measured isobaric charge distributions. Parameters used in this parametrization have been obtained by comparing with many experimental data. Quantitative investigations demonstrate that this parametrization agrees well with most experimental isotopic yields within a factor of 1.6 and thus can provide accurate calculations for production cross sections of neutron-rich fragments produced by ^{238}U photofission. This parametrization has also been applied to check isotopic yields measured in a most recent experiment of ^{238}U photofission induced by virtual photons, where the background induced by fragmentation is found to be improperly subtracted. More photofission experimental data without background are needed to validate and improve the GIF^{238}U parametrization. Finally, production cross sections of photofission fragments calculated by this parametrization reveal that ^{238}U photofission is very suitable for producing many neutron-rich exotic nuclei with $31 \leqslant Z \leqslant 62$ and $80 \leqslant A \leqslant 160$, which are on or very close to the r-process path. Production rates of some neutron-rich fragments produced by photofission of ^{238}U are estimated for the planned IGISOL facility at ELI-NP.

ACKNOWLEDGMENTS

This research was supported by the Extreme Light Infrastructure Nuclear Physics (ELI-NP) Phase II, a project cofinanced by the Romanian Government and the European Union through the European Regional Development Fund's Competitiveness Operational Programme (1/07.07.2016, COP, ID 1334). P.V.C. and L.T.A. would like to acknowledge the support from the Vietnam Academy of Science and Technology under Grant No. VAST. CTVL.03/17-18.

[1] J. T. Caldwell, E. J. Dowdy, B. L. Berman, R. A. Alvarez, and P. Meyer, Phys. Rev. C **21**, 1215 (1980).
[2] H. Ries, G. Mank, J. Drexler, R. Heil, K. Huber, U. Kneissl, R. Ratzek, H. Ströher, T. Weber, and W. Wilke, Phys. Rev. C **29**, 2346 (1984).
[3] L. Csige, D. M. Filipescu, T. Glodariu, J. Gulyás, M. M. Günther, D. Habs, H. J. Karwowski, A. Krasznahorkay, G. C. Rich, M. Sin, L. Stroe, O. Tesileanu, and P. G. Thirolf, Phys. Rev. C **87**, 044321 (2013).
[4] A. Veyssière, H. Beil, R. Bergère, P. Carlos, A. Lepretre, and K. Kernbath, Nucl. Phys. A **199**, 45 (1973).
[5] E. Jacobs, H. Thierens, D. De Frenne, A. De Clercq, P. D'hondt, P. De Gelder, and A. J. Deruytter, Phys. Rev. C **19**, 422 (1979).
[6] S. S. Belyshev, B. S. Ishkhanov, A. A. Kuznetsov, and K. A. Stopani, Phys. Rev. C **91**, 034603 (2015).
[7] D. De Frenne, H. Thierens, B. Proot, E. Jacobs, P. De Gelder, and A. De Clercq, Phys. Rev. C **29**, 1908 (1984).
[8] D. L. Balabanski *et al.*, Rom. Rep. Phys. **68**, S621 (2016).
[9] U. Brosa, S. Grossmann, and A. Müller, Phys. Rep. **197**, 167 (1990).
[10] W. T. Diamond, Nucl. Instrum. Methods Phys. Res., Sect. A **432**, 471 (1999).
[11] M. C. Mhamed *et al.*, Nucl. Instrum. Methods Phys. Res., Sect. B **266**, 4092 (2008).
[12] Y. T. Oganessian, S. N. Dmitriev, J. Kliman, O. A. Maslov, G. Y. Starodub, A. G. Belov, and S. P. Tretiakova, Nucl. Phys. A **701**, 87 (2002).
[13] G. C. Ball, G. Hackman, and R. Krücken, Phys. Scr. **91**, 093002 (2016).

[14] A. Chakrabarti, A. Bandyopadhyay, V. Naik, S. Dechoudhury, M. Mondal, and P. Y. Nabhiraj, Nucl. Instrum. Methods Phys. Res., Sect. B **317**, 253 (2013).
[15] P. Constantin, D. L. Balabanski, and P. V. Cuong, Nucl. Instrum. Methods Phys. Res., Sect. B **372**, 78 (2016).
[16] P. Constantin, D. L. Balabanski, L. T. Anh, P. V. Cuong, and B. Mei, Nucl. Instrum. Methods Phys. Res., Sect. B **397**, 1 (2017).
[17] H. Naik, S. V. Suryanarayana, K. C. Jagadeesan, S. V. Thakare, P. V. Joshi, V. T. Nimje, K. C. Mittal, A. Goswami, V. Venugopal, and S. Kailas, J. Radioanal. Nucl. Chem. **295**, 807 (2013).
[18] D. J. S. Findlay, Nucl. Instrum. Methods Phys. Res., Sect. B **50**, 314 (1990).
[19] K.-H. Schmidt, B. Jurado, C. Amouroux, and C. Schmitt, Nucl. Data Sheets **131**, 107 (2016).
[20] V. Rubchenya and J. Äystö, Eur. Phys. J. A **48**, 44 (2012).
[21] D. Bhowmick, D. Atta, D. N. Basu, and A. Chakrabarti, Phys. Rev. C **91**, 044611 (2015).
[22] F. A. Khan, D. Bhowmick, D. N. Basu, M. Farooq, and A. Chakrabarti, Phys. Rev. C **94**, 054605 (2016).
[23] E. Dupont *et al.*, in *Proceedings of the International Conference on Nuclear Data for Science and Technology, 2007, Nice, France*, edited by O. Bersillon, F. Gunsing, E. Bauge, R. Jacqmin, and S. Leray (EDP Sciences, Les Ulis, France, 2007), article 181.
[24] C. Donzaud *et al.*, Eur. Phys. J. A **1**, 407 (1998).
[25] D. De Frenne, H. Thierens, E. Jacobs, P. De Gelder, A. De Clercq, P. D'hondt, and A. J. Deruytter, Phys. Rev. C **21**, 629 (1980).
[26] S. Pommé, E. Jacobs, K. Persyn, D. De Frenne, K. Govaert, and M.-L. Yoneama, Nucl. Phys. A **560**, 689 (1993).
[27] P. R. Chowdhury and D. N. Basu, Acta Phys. Pol., B **37**, 1833 (2006).
[28] E. Pellereau, J. Taïeb, A. Chatillon, H. Alvarez-Pol, L. Audouin, Y. Ayyad, G. Bélier, J. Benlliure, G. Boutoux, M. Caamaño, E. Casarejos, D. Cortina-Gil, A. Ebran, F. Farget, B. Fernández-Domínguez, T. Gorbinet, L. Grente, A. Heinz, H. Johansson, B. Jurado, A. Kelić-Heil, N. Kurz, B. Laurent, J. F. Martin, C. Nociforo, C. Paradela, S. Pietri, J. L. Rodríguez-Sánchez, K.-H. Schmidt, H. Simon, L. Tassan-Got, J. Vargas, B. Voss, and H. Weick, Phys. Rev. C **95**, 054603 (2017).
[29] B. Mei, Phys. Rev. C **95**, 034608 (2017).
[30] T. Rauscher, F. K. Thielemann, and K. L. Kratz, Phys. Rev. C **56**, 1613 (1997).
[31] S. Goriely, S. Hilaire, and A. J. Koning, Phys. Rev. C **78**, 064307 (2008).
[32] H. Penttilä *et al.*, Eur. Phys. J. Spec. Top. **150**, 317 (2007).
[33] H. Penttilä *et al.*, Eur. Phys. J. A **48**, 43 (2012).
[34] H. Schatz and K. Blaum, Europhys. News **37**, 16 (2006).
[35] T. Kurtukian-Nieto *et al.*, Phys. Rev. C **89**, 024616 (2014).
[36] D. Henzlova, K.-H. Schmidt, M. V. Ricciardi, A. Kelić, V. Henzl, P. Napolitani, L. Audouin, J. Benlliure, A. Boudard, E. Casarejos, J. E. Ducret, T. Enqvist, A. Heinz, A. Junghans, B. Jurado, A. Krása, T. Kurtukian, S. Leray, M. F. Ordóñez, J. Pereira, R. Pleskač, F. Rejmund, C. Schmitt, C. Stéphan, L. Tassan-Got, C. Villagrasa, C. Volant, A. Wagner, and O. Yordanov, Phys. Rev. C **78**, 044616 (2008).
[37] O. B. Tarasov, M. Portillo, D. J. Morrissey, A. M. Amthor, L. Bandura, T. Baumann, D. Bazin, J. S. Berryman, B. A. Brown, G. Chubarian, N. Fukuda, A. Gade, T. N. Ginter, M. Hausmann, N. Inabe, T. Kubo, J. Pereira, B. M. Sherrill, A. Stolz, C. Sumithrarachichi, M. Thoennessen, and D. Weisshaar, Phys. Rev. C **87**, 054612 (2013).
[38] B. Mei, H. S. Xu, X. L. Tu, Y. H. Zhang, Y. A. Litvinov, K.-H. Schmidt, M. Wang, Z. Y. Sun, X. H. Zhou, Y. J. Yuan, M. V. Ricciardi, A. Kelić-Heil, R. Reifarth, K. Blaum, R. S. Mao, Z. G. Hu, P. Shuai, Y. D. Zang, X. W. Ma, X. Y. Zhang, J. W. Xia, G. Q. Xiao, Z. Y. Guo, J. C. Yang, X. H. Zhang, X. Xu, X. L. Yan, W. Zhang, and W. L. Zhan, Phys. Rev. C **89**, 054612 (2014).
[39] B. Mei, H. S. Xu, Y. H. Zhang, M. Wang, X. L. Tu, K.-H. Schmidt, Y. A. Litvinov, Z. Y. Sun, X. H. Zhou, Y. J. Yuan, K. Blaum, M. V. Ricciardi, A. Kelić-Heil, R. S. Mao, Z. G. Hu, P. Shuai, Y. D. Zang, X. W. Ma, X. Y. Zhang, J. W. Xia, G. Q. Xiao, Z. Y. Guo, J. C. Yang, X. H. Zhang, X. Xu, X. L. Yan, W. Zhang, and W. L. Zhan, Phys. Rev. C **94**, 044615 (2016).